

Crystal structure of givinostat hydrochloride monohydrate Form I, $C_{24}H_{28}N_3O_4Cl(H_2O)$

James A. Kaduk^{1,2} , Anja Dosen³  and Tom Blanton³ 

¹Department of Chemistry, Illinois Institute of Technology, 3101 South Dearborn Street, Chicago, IL 60616, USA

²Department of Physics, North Central College, 131 South Loomis Street, Naperville, IL 60540, USA

³International Centre for Diffraction Data (ICDD), 12 Campus Boulevard, Newtown Square, PA 19073-3273, USA

(Received 28 December 2024; revised 15 April 2025; accepted 22 April 2025)

Abstract: The crystal structure of givinostat hydrochloride monohydrate Form I has been solved and refined using synchrotron X-ray powder diffraction data and optimized using density functional theory techniques. Givinostat hydrochloride monohydrate Form I crystallizes in the space group $P2_1$ (#4) with $a = 7.98657(17)$, $b = 8.20633(10)$, $c = 18.2406(6)$ Å, $\beta = 98.1069(13)^\circ$, $V = 1,183.55(4)$ Å³, and $Z = 2$ at 298 K. The crystal structure consists of layers of cations and anions/water molecules parallel to the ab -plane. The cations stack along the a -axis, with the phenyl and naphthalene rings alternating in the stacks. Hydrogen bonds link the cations, anions, and water molecules in two-dimensional networks parallel to the ab -plane. The powder pattern has been submitted to the International Centre for Diffraction Data for inclusion in the Powder Diffraction File™ (PDF®).

© The Author(s), 2025. Published by Cambridge University Press on behalf of International Centre for Diffraction Data. This is an Open Access article, distributed under the terms of the Creative Commons Attribution licence (<http://creativecommons.org/licenses/by/4.0>), which permits unrestricted re-use, distribution and reproduction, provided the original article is properly cited. [doi:10.1017/S0885715625100559]

Key words: givinostat, Duvyzat™, crystal structure, Rietveld refinement, density functional theory

I. INTRODUCTION

Givinostat (as the hydrochloride, sold under the brand name Duvyzat) is used for the treatment of Duchenne muscular dystrophy. Givinostat functions by inhibiting histone deacetylases that can reduce muscle regeneration. Treatment using Duvyzat can help promote muscle repair and muscle fiber generation, and reduce inflammation and fibrosis. The systematic name (CAS Registry No. 199657-29-9) is [6-(diethylaminomethyl)naphthalen-2-yl]methyl N-[4-(hydroxycarbonyl)phenyl]carbamatehydrochloride hydrate. A two-dimensional molecular diagram of givinostat hydrochloride monohydrate is shown in Figure 1.

Synthesis of givinostat is described in U.S. Patent 6034096 (Bertolini et al., 2000; Italfarmaco). A novel crystalline givinostat hydrochloride monohydrate is claimed in U.S. Patent 7329689 (Pinori and Mascagni, 2008; Italfarmaco). It is described as advantageous for industrial use as it is more stable and easier to handle than anhydrous givinostat. A novel crystalline Form II of givinostat hydrochloride monohydrate is claimed in International Patent Application WO 2011/092556 (Turchetta and Zenoni, 2011; Chemi SPA).

This work was carried out as part of a project (Kaduk et al., 2014) to determine the crystal structures of large-volume commercial pharmaceuticals and include high-quality powder diffraction data for them in the Powder Diffraction File™ (Kabekkodu et al., 2024).

II. EXPERIMENTAL

Givinostat hydrochloride monohydrate was a commercial reagent, purchased from TargetMol (Batch #T6279), and was used as received. The orange/tan powder was packed into a 0.5-mm-diameter Kapton capillary and rotated during the measurement at ~2 Hz. The powder pattern was measured at 298(1) K at the Wiggler Low Energy Beamline (Leontowich et al., 2021) of the Brockhouse X-ray Diffraction and Scattering Sector of the Canadian Light Source using a wavelength of 0.819826(2) Å (15.1 keV) from 1.6 to 75.0° 2θ with a step size of 0.0025° and a collection time of 3 minutes. The high-resolution powder diffraction data were collected using eight Dectris Mythen2 X series 1K linear strip detectors. NIST SRM 660b LaB₆ was used to calibrate the instrument and refine the monochromatic wavelength used in the experiment.

The pattern was indexed using N-TREOR as incorporated into EXPO2014 (Altomare et al., 2013) on a primitive monoclinic unit cell with $a = 7.99633$, $b = 8.20718$, $c = 18.22845$ Å, $\beta = 98.138^\circ$, $V = 1,184.2$ Å³, and $Z = 2$. The suggested space group was $P2_1$, which was confirmed by the successful solution and refinement of the structure. A reduced cell search of the Cambridge Structural Database (Groom et al., 2016) yielded 15 hits, but no structures of givinostat or its derivatives.

A neutral givinostat molecule was downloaded from PubChem (Kim et al., 2023) as Conformer3D_COMPOUND_CID_9804992.sdf. It was converted to a *.mol2 file using Mercury (Macrae et al., 2020). The crystal structure was solved using Monte Carlo-simulated annealing techniques as implemented in EXPO2014 (Altomare et al., 2013), using a

Corresponding author: James A. Kaduk; Email: kaduk@polycrystallography.com



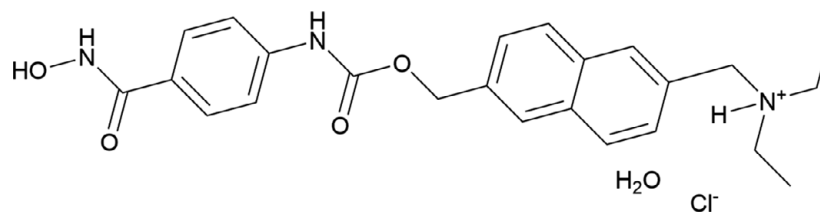


Figure 1. The two-dimensional structure of givinostat hydrochloride monohydrate.

givinostat molecule, a Cl atom, and an O atom as fragments, with (001) preferred orientation and a bump penalty. In the best solution, the tertiary nitrogen atom N5 was 3.100 Å from the Cl atom (as expected from the patents); therefore, a hydrogen atom was added to it. The O atom was in a position to be the acceptor in a N–H···O hydrogen bond and a donor in two O–H···Cl hydrogen bonds; therefore, two approximate water hydrogen positions were generated along the O···Cl vectors using Materials Studio (Dassault Systèmes, 2023). The position of the hydroxyl proton H58 was recalculated to lie along an O···Cl vector.

Rietveld refinement was carried out with GSAS-II (Toby and Von Dreele, 2013). Only the 2.0–50.0° portion of the pattern was included in the refinements ($d_{\min} = 0.970$ Å). The initial fit and the appearance of the high-angle portion of the pattern made it clear that an impurity phase was present. It was identified as NaCl, which was added to the refinement as a second phase. Its concentration refined to 1.0 wt%. The y-coordinate of O1 was fixed to define the origin. All non-H-bond distances and angles were subjected to restraints, based on a Mercury/Mogul Geometry Check (Bruno et al., 2004; Sykes et al., 2011). The Mogul average and standard deviation for each quantity were used as the restraint parameters. The benzene and naphthalene ring systems were restrained to be planar. The restraints contributed 2.5% to the overall χ^2 . The

hydrogen atoms were included in calculated positions, which were recalculated during the refinement using Materials Studio (Dassault Systèmes, 2023). The U_{iso} values of the heavy atoms were grouped by chemical similarity. The U_{iso} values of the H atoms were fixed at 1.3× those of the heavy atoms to which they are attached. The thermal motion of the Cl atom was described by an anisotropic model. The peak profiles were described using the generalized (Stephens, 1999) micro-strain model. The background was modeled using a six-term shifted Chebyshev polynomial, with peaks at 2.89 and 10.86° to model the narrow and broad scattering from the Kapton capillary and any amorphous component.

The final refinement of 141 variables using 19,201 observations and 79 restraints yielded the residual $R_{\text{wp}} = 0.04917$. The largest peak (1.04 Å from C12) and hole (1.42 Å from O3) in the difference Fourier map were 0.37(10) and $-0.44(10) e\text{Å}^{-3}$, respectively. The final Rietveld plot is shown in Figure 2. The largest features in the normalized error plot are in the asymmetry and shape of the lowest-angle peak and the shapes of some of the strong low-angle peaks. These misfits probably indicate subtle changes in the specimen during the measurement.

The crystal structure of givinostat hydrochloride monohydrate was optimized (fixed experimental unit cell) with density functional techniques using VASP (Kresse and

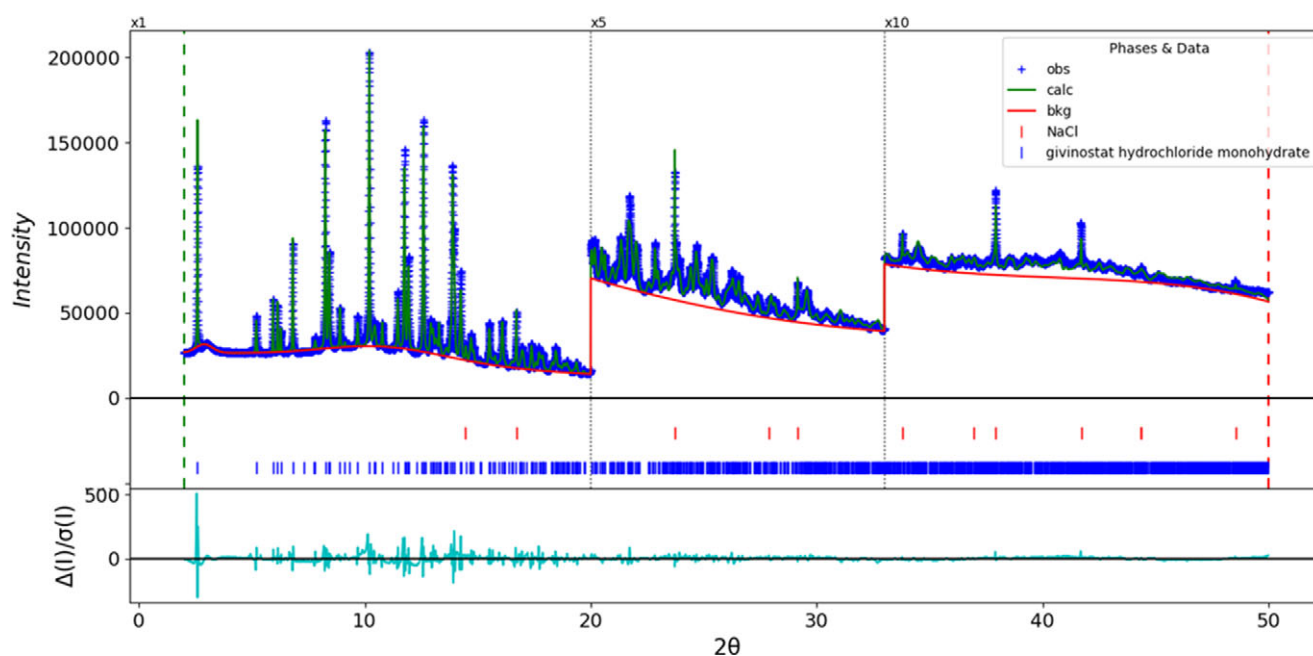


Figure 2. The Rietveld plot for givinostat hydrochloride monohydrate Form I. The blue crosses represent the observed data points, and the green line represents the calculated pattern. The cyan curve indicates the normalized error plot, and the red line indicates the background curve. The blue tick marks indicate the givinostat hydrochloride monohydrate peak positions, and the red tick marks indicate those of NaCl. The vertical scale has been multiplied by a factor of 5× for $2\theta > 20.0$ and by a factor of 10× for $2\theta > 33.0$.

Furthmüller, 1996) through the MedeA graphical interface (Materials Design, 2024). The calculation was carried out on 32 cores of a 144-core (768-GB memory) HPE Superdome Flex 280 Linux server at North Central College. The calculation used the GGA-PBE functional, a plane wave cutoff energy of 400.0 eV, and a k -point spacing of 0.5 \AA^{-1} , leading to a $2 \times 2 \times 1$ mesh and took approximately 2.0 hours. Single-point density functional calculations (fixed experimental cell) and population analysis were carried out using CRYSTAL23 (Erba et al., 2023). The basis sets for the H, C, and O atoms in the calculation were those of Gatti et al. (1994), whereas for Cl, the basis set was that of Peintinger et al. (2013). The calculations were run on a 3.5-GHz PC using eight k -points and the B3LYP functional and took approximately 3.2 hours.

III. RESULTS AND DISCUSSION

This synchrotron powder pattern of givinostat hydrochloride monohydrate (Figure 3) matches the one reported for Form I by Pinori and Mascagni (2008) well enough to conclude that they represent the same material, and thus that our sample is Form I.

The root-mean-square (rms) difference of the non-H atoms in the Rietveld-refined and VASP-optimized structures, calculated using the Mercury CSD-Materials/Search/Crystal Packing Similarity tool, is 0.097 \AA . The rms Cartesian displacement of the non-H atoms in the Rietveld-refined and VASP-optimized structures of the cation, calculated using the Mercury Calculate/Molecule Overlay tool, is 0.085 \AA (Figure 4). The agreements are within the normal range for correct structures (van de Streek and Neumann, 2014). The asymmetric unit is illustrated in Figure 5. The remaining discussion will emphasize the VASP-optimized structure.

All of the bond distances, bond angles, and torsion angles fall within the normal ranges indicated by a Mercury Mogul Geometry check (Macrae et al., 2020). Quantum chemical

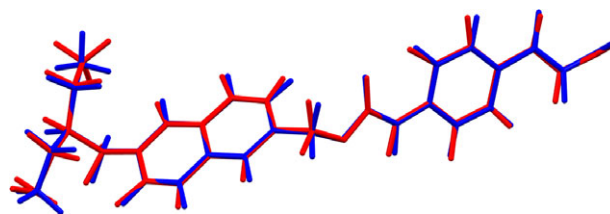


Figure 4. Comparison of the Rietveld-refined (red) and VASP-optimized (blue) structures of the cation in givinostat hydrochloride monohydrate Form I. The root-mean-square Cartesian displacement is 0.085 \AA . Image generated using Mercury (Macrae et al., 2020).

geometry optimizations of isolated givinostat cations (DFT/B3LYP/6-31G*/water) using Spartan '24 (Wavefunction, Inc., 2023) indicated that the observed conformation is 5.7 kcal/mol higher in energy than a local minimum, but very similar in geometry. The global minimum-energy conformation (MMFF force field) is only 3.2 kcal/mol lower in energy but is very different than the observed conformation (rms displacement = 1.916 \AA). Intermolecular interactions are thus important in determining the solid-state conformation.

The crystal structure (Figure 6) consists of layers of cations and anions/water molecules parallel to the ab -plane. The cations stack along the a -axis, with the phenyl and naphthalene rings alternating in the stacks. Hydrogen bonds (discussed below) link the cations, anions, and water molecules. The mean planes of the phenyl and naphthalene ring systems are approximately (1, -13, 17) and (2, 7, 13). The Mercury Aromatics Analyser indicates one strong interaction between the phenyl and naphthalene rings, with a distance of 4.02 \AA , as well as several moderate interactions with distances ranging from 5.36 to 6.11 \AA .

Analysis of the contributions to the total crystal energy of the structure using the Forcite module of Materials Studio (Dassault Systèmes, 2023) indicates that the intramolecular

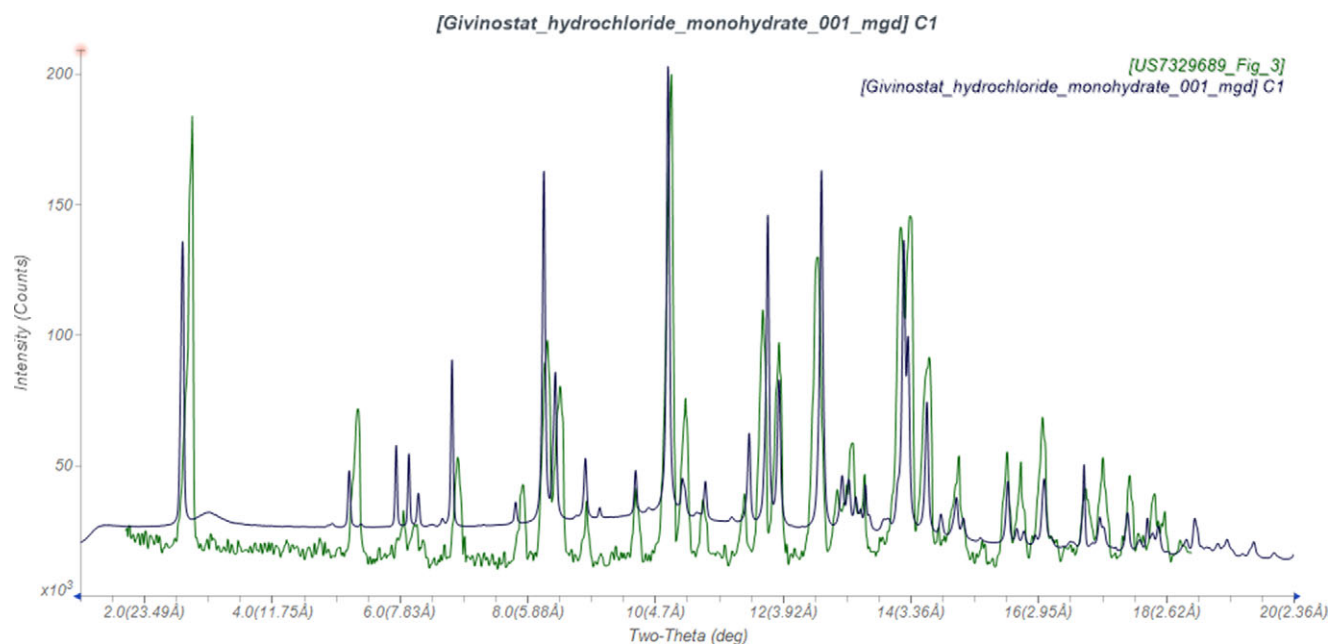


Figure 3. Comparison of the synchrotron pattern of givinostat hydrochloride monohydrate Form I (black) to that reported by Pinori and Mascagni (2008) (green). The literature pattern (measured using $\text{Cu K}\alpha$ radiation) was digitized using UN-SCAN-IT (Silk Scientific, 2013) and converted to the synchrotron wavelength of $0.819826(2) \text{ \AA}$ using JADE Pro (MDI, 2024). Image generated using JADE Pro (MDI, 2024).

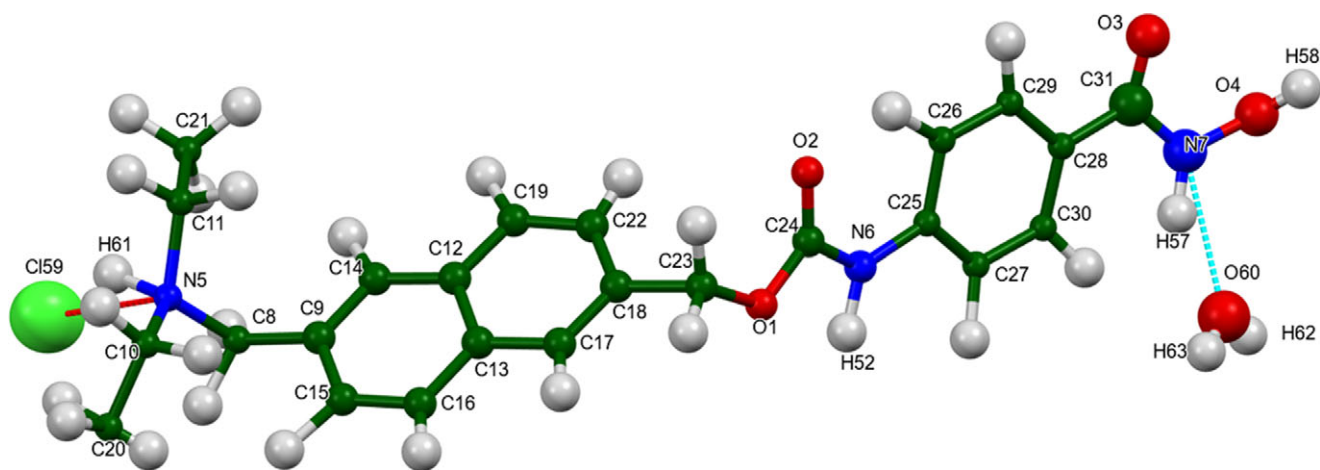


Figure 5. The asymmetric unit of givinostat hydrochloride monohydrate Form I, with the atom numbering. The atoms are represented by 50% probability spheroids/ellipsoids. Image generated using Mercury (Macrae et al., 2020).

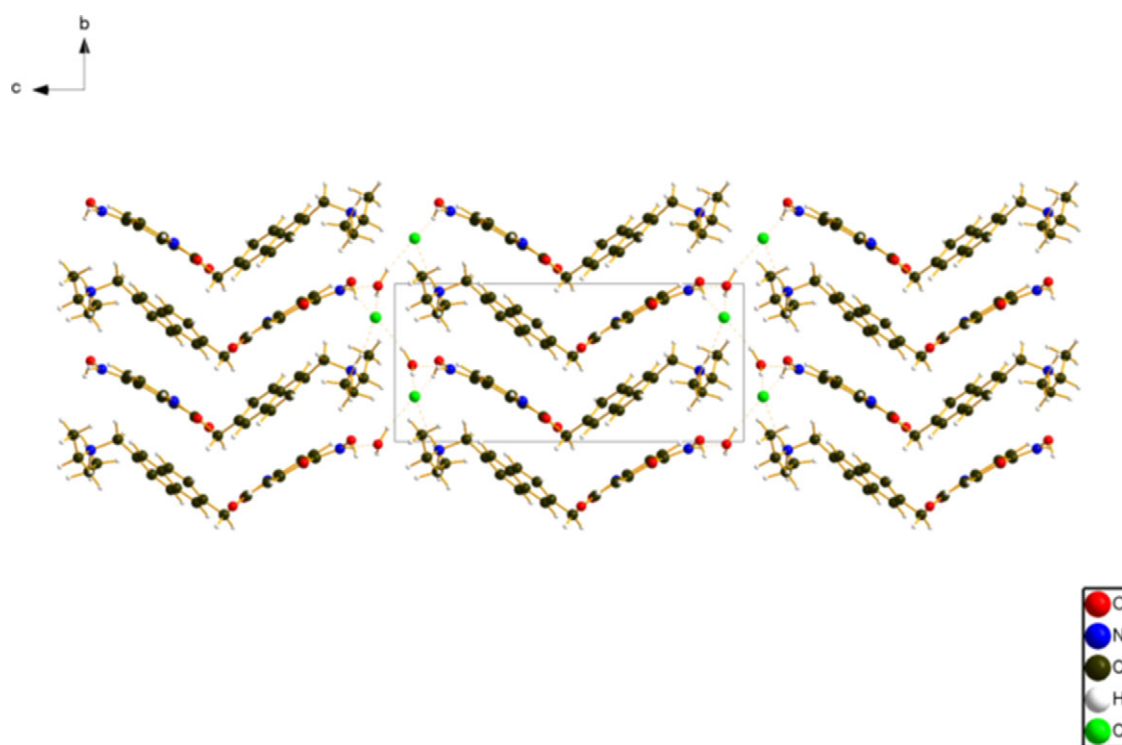


Figure 6. The crystal structure of givinostat hydrochloride monohydrate Form I, viewed down the *a*-axis. Image generated using Diamond (Crystal Impact, 2023).

energy is fairly small, and that bond, angle, and torsion distortion terms contribute significantly. The intermolecular energy is dominated by electrostatic attractions, which, in this force field-based analysis, also include hydrogen bonds. The hydrogen bonds are better discussed using the results of the density functional theory (DFT) calculation.

The water molecule, the hydroxylamino group, and the protonated N atom all form strong hydrogen bonds to the chloride anion (Table I). Both amino groups N7 and N6 act as donors in N–H···O hydrogen bonds, to the water molecule and carbonyl groups, respectively. The energies of the N–H···O hydrogen bonds were calculated using the correlation of Wheatley and Kaduk (2019). The N6–H52···O3 hydrogen bonds link the cations into a chain with a graph set $C1, I(8)$

(Etter, 1990; Bernstein et al., 1995; Motherwell et al., 2000). The other hydrogen bonds are discrete but result in two-dimensional networks of hydrogen bonds linking the cations, anions, and water molecules parallel to the *ab*-plane. There are several C–H···O hydrogen bonds from the cations to the water molecules, as well as between cations. C–H···Cl and one C–H···C interactions also contribute to the lattice energy.

The Hirshfeld surface for givinostat hydrochloride monohydrate (Hirshfeld, 1977; Spackman et al., 2021) is shown in Figure 7. The volume is 581.56 Å³, 98.27% of half the unit cell volume. The packing density is thus typical. The only significant close contacts (red in Figure 7) involve the hydrogen bonds. The volume/non-hydrogen atom is typical at 17.9 Å³.

TABLE I. Hydrogen bonds (CRYSTAL23) in givinostat hydrochloride monohydrate

H-bond	D–H, Å	H…A, Å	D…A, Å	D–H…A, °	Mulliken overlap, <i>e</i>	<i>E</i> , kcal/mol
O60–H63…C159	0.991	2.136	3.124	173.9	0.066	
O60–H62…C159	0.990	2.145	3.112	164.9	0.062	
N5–H61…C159	1.055	2.140	3.172	165.3	0.079	
O4–H58…C159	0.997	2.188	3.128	156.4	0.060	
N7–H57…O60	1.038	1.770	2.792	167.7	0.065	5.9
N6–H52…O3	1.035	1.820	2.823	162.2	0.057	5.5
C30–H56…O60	1.090	2.472	3.416	144.3	0.018	
C20–H44…O60	1.098	2.750	3.727	148.1	0.011	
C10–H35…O60	1.097	2.669	3.394	123.0	0.010	
C29–H55…O1	1.090	2.392	3.461	166.7	0.019	
C26–H53…O2	1.087	2.208 ^a	2.904	119.7	0.016	
C23–H51…O2	1.099	2.256 ^a	2.744	104.3	0.021	
C10–H34…O4	1.099	2.567	3.371	129.2	0.011	
C8–H32…O3	1.096	2.362	3.313	144.0	0.023	
C21–H47…C159	1.099	2.880	3.706	132.0	0.013	
C21–H46…C159	1.099	2.857	3.879	154.8	0.022	
C11–H37…C9	1.097	2.722 ^a	3.099	99.6	0.010	

^aIntramolecular.

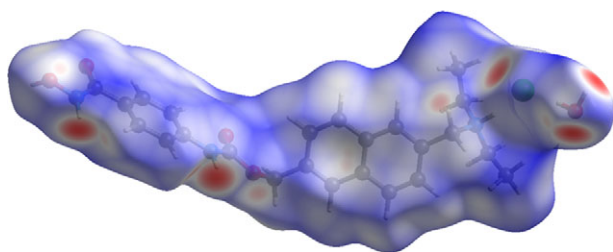


Figure 7. The Hirshfeld surface of givinostat hydrochloride monohydrate Form I. Intermolecular contacts longer than the sums of the van der Waals radii are colored blue, and contacts shorter than the sums of the radii are colored red. Contacts equal to the sums of radii are white. Image generated using CrystalExplorer (Spackman et al., 2021).

The Bravais–Friedel–Donnay–Harker (Bravais, 1866; Friedel, 1907; Donnay and Harker, 1937) algorithm suggests that we might expect platy morphology for givinostat hydrochloride monohydrate, with {001} as the major faces. A second-order spherical harmonic model was included in the refinement. The texture index (calculated from the refined harmonic coefficients) was 1.007(0), indicating that the preferred orientation was insignificant in this rotated capillary specimen.

ACKNOWLEDGEMENTS

We thank Adam Leontowich for his assistance in the data collection. We also thank the ICDD team – Megan Rost, Steve Trimble, and Dave Bohnenberger – for their contribution to research, sample preparation, and in-house XRD data collection and verification.

DATA AVAILABILITY STATEMENT

The powder pattern of givinostat hydrochloride monohydrate Form I from this synchrotron dataset has been submitted to the International Centre for Diffraction Data (ICDD) for inclusion in the Powder Diffraction File. The Crystallographic Information Framework (CIF) files containing the results of

the Rietveld refinement (including the raw data) and the DFT geometry optimization were deposited with the ICDD. The data can be requested at pdj@icdd.com.

FUNDING STATEMENT

Part or all of the research described in this paper was performed at the Canadian Light Source, a national research facility of the University of Saskatchewan, which is supported by the Canada Foundation for Innovation (CFI), the Natural Sciences and Engineering Research Council (NSERC), the Canadian Institute of Health Research (CIHR), the Government of Saskatchewan, and the University of Saskatchewan. This work was partially supported by the International Centre for Diffraction Data (ICDD).

CONFLICTS OF INTEREST

The authors have no conflicts of interest to declare.

REFERENCES

- Altomare, A., C. Cuocci, C. Giacovazzo, A. Moliterni, R. Rizzi, N. Corriero, and A. Falcicchio. 2013. “EXPO2013: A Kit of Tools for Phasing Crystal Structures from Powder Data.” *Journal of Applied Crystallography* 46: 1231–35.
- Bernstein, J., R. E. Davis, L. Shimoni, and N. L. Chang. 1995. “Patterns in Hydrogen Bonding: Functionality and Graph Set Analysis in Crystals.” *Angewandte Chemie International Edition in English* 34: 1555–73.
- Bertolini, G., M. Biffi, F. Leoni, J. Mizrahi, G. Pavich, and P. Mascagni. 2000. “Compounds with Anti-Inflammatory and Immunosuppressive Activities.” U.S. Patent 6034096.
- Bravais, A. 1866. *Etudes Cristallographiques*. Gauthier Villars.
- Bruno, I. J., J. C. Cole, M. Kessler, J. Luo, W. D. S. Motherwell, L. H. Purkis, B. R. Smith, et al. 2004. “Retrieval of Crystallographically Derived Molecular Geometry Information.” *Journal of Chemical Information and Computer Sciences* 44: 2133–44.
- Crystal Impact. 2023. *Diamond V. 5.0.0*. Crystal Impact – Dr. H. Putz & Dr. K. Brandenburg.
- Dassault Systèmes. 2023. *BIOVIA Materials Studio 2024*. BIOVIA.
- Donnay, J. D. H., and D. Harker. 1937. “A New Law of Crystal Morphology Extending the Law of Bravais.” *American Mineralogist* 22: 446–67.
- Erba, A., J. K. Desmarais, S. Casassa, B. Civalieri, L. Donà, I. J. Bush, B. Searle, et al. 2023. “CRYSTAL23: A Program for Computational Solid

- State Physics and Chemistry.” *Journal of Chemical Theory and Computation* 19: 6891–932. <https://doi.org/10.1021/acs.jctc.2c00958>.
- Etter, M. C. 1990. “Encoding and Decoding Hydrogen-Bond Patterns of Organic Compounds.” *Accounts of Chemical Research* 23: 120–26.
- Friedel, G. 1907. “Etudes sur la loi de Bravais.” *Bulletin de la Société Française de Minéralogie* 30: 326–455.
- Gatti, C., V. R. Saunders, and C. Roetti. 1994. “Crystal-Field Effects on the Topological Properties of the Electron-Density in Molecular Crystals – the Case of Urea.” *Journal of Chemical Physics* 101: 10686–96.
- Groom, C. R., I. J. Bruno, M. P. Lightfoot, and S. C. Ward. 2016. “The Cambridge Structural Database.” *Acta Crystallographica Section B: Structural Science, Crystal Engineering and Materials* 72: 171–79.
- Hirshfeld, F. L. 1977. “Bonded-Atom Fragments for Describing Molecular Charge Densities.” *Theoretica Chimica Acta* 44: 129–38.
- Kabekkodu, S., A. Dosen, and T. N. Blanton. 2024. “PDF-5+; A Comprehensive Powder Diffraction File™ for Materials Characterization.” *Powder Diffraction* 39: 47–59.
- Kaduk, J. A., C. E. Crowder, K. Zhong, T. G. Fawcett, and M. R. Suchomel. 2014. “Crystal Structure of Atomoxetine Hydrochloride (Strattera), C₁₇H₂₂NOCl.” *Powder Diffraction* 29: 269–73.
- Kim S., J. Chen, T. Cheng, A. Gindulyte, J. He, S. He, Q. Li, et al. 2023. “PubChem 2023 Update.” *Nucleic Acids Research* 51 (D1): D1373–80. <https://doi.org/10.1093/nar/gkac956>.
- Kresse, G., and J. Furthmüller. 1996. “Efficiency of Ab-Initio Total Energy Calculations for Metals and Semiconductors Using a Plane-Wave Basis Set.” *Computational Materials Science* 6: 15–50.
- Leontowich, A. F. G., A. Gomez, B. Diaz Moreno, D. Muir, D. Spasyuk, G. King, J. W. Reid, C.-Y. Kim, and S. Kycia. 2021. “The Lower Energy Diffraction and Scattering Side-Bounce Beamline for Materials Science at the Canadian Light Source.” *Journal of Synchrotron Radiation* 28: 1–9. <https://doi.org/10.1107/S1600577521002496>.
- Macrae, C. F., I. Sovago, S. J. Cottrell, P. T. A. Galek, P. McCabe, E. Pidcock, M. Platings, et al. 2020. “Mercury 4.0: From Visualization to Design and Prediction.” *Journal of Applied Crystallography* 53: 226–35.
- Materials Design. 2024. *MedeA 3.7.2*. Materials Design, Inc.
- MDI. 2024. *JADE Pro Version 9.0*. Materials Data.
- Motherwell, W. D. S., G. P. Shields, and F. H. Allen. 2000. “Graph-Set and Packing Analysis of Hydrogen-Bonded Networks in Polyamide Structures in the Cambridge Structural Database.” *Acta Crystallographica B* 56: 857–71.
- Peintinger, M. F., D. Vilela Oliveira, and T. Bredow. 2013. “Consistent Gaussian Basis Sets of Triple-Zeta Valence with Polarization Quality for Solid-State Calculations.” *Journal of Computational Chemistry* 34: 451–59.
- Pinori, M., and P. Mascagni. 2008. “Monohydrate Hydrochloride of the 4-Hydroxycarbamoylphenyl)-Carbamic Acid (6-Diethylaminomethylnaphtalen-2-Yl) Ester.” U.S. Patent 7329689 B2.
- Silk Scientific. 2013. *UN-SCAN-IT 7.0*. Silk Scientific Corporation.
- Spackman, P. R., M. J. Turner, J. J. McKinnon, S. K. Wolff, D. J. Grimwood, D. Jayatilaka, and M. A. Spackman. 2021. “CrystalExplorer: A Program for Hirshfeld Surface Analysis, Visualization and Quantitative Analysis of Molecular Crystals.” *Journal of Applied Crystallography* 54: 1006–11. <https://doi.org/10.1107/S1600577521002910>; <https://crystalexplorer.net>.
- Stephens, P. W. 1999. “Phenomenological Model of Anisotropic Peak Broadening in Powder Diffraction.” *Journal of Applied Crystallography* 32: 281–89.
- Sykes, R. A., P. McCabe, F. H. Allen, G. M. Battle, I. J. Bruno, and P. A. Wood. 2011. “New Software for Statistical Analysis of Cambridge Structural Database Data.” *Journal of Applied Crystallography* 44: 882–86.
- Toby, B. H., and R. B. Von Dreele. 2013. “GSAS II: The Genesis of a Modern Open Source All Purpose Crystallography Software Package.” *Journal of Applied Crystallography* 46: 544–49.
- Turchetta, S., and M. Zenoni. 2011. “Novel Polymorph of the Hydrochloride of the 4-Hydroxycarbamoylphenyl)-Carbamic Acid (6-Diethylaminomethylnaphtalen-2-Yl) Ester.” International Patent Application WO 2011/092556 A1.
- van de Streek, J., and M. A. Neumann. 2014. “Validation of Molecular Crystal Structures from Powder Diffraction Data with Dispersion-Corrected Density Functional Theory (DFT-D).” *Acta Crystallographica Section B: Structural Science, Crystal Engineering and Materials* 70: 1020–32.
- Wavefunction, Inc. 2023. *Spartan '24. V. 1.0.0*. Wavefunction, Inc.
- Wheatley, A. M., and J. A. Kaduk. 2019. “Crystal Structures of Ammonium Citrates.” *Powder Diffraction* 34: 35–43.